COMPARISON OF NUMERICAL AND EXPERIMENTAL PERFORMANCE CRITERIA OF AN AMMONIA-WATER BUBBLE ABSORBER USING PLATE HEAT EXCHANGERS

Jesús Cerezo[a*], Roberto Best[a], Mahmoud Bourouis[b], Alberto Coronas[b]

[a]Centro de Investigación en Energía, Universidad Nacional Autónoma de México, Privada Xochicalco s/n, Temixco, Morelos, 62580, México.

[b]CREVER-Universitat Rovira i Virgili, Av. Països Catalans No. 26, 43007, Tarragona, España

ABSTRACT

A mathematical model for ammonia-water bubble absorbers was developed and compared with experimental data using a plate heat exchanger. The analysis was performed carrying out a sensitive study of selected operation parameters on the absorber thermal load and mass absorption flux. Regarding the experimental data, the values obtained for the solution heat transfer were in the range 0.51–1.21 kW/m^{2}K and those of the mass absorption flux in the range 2.5-5.0x10^{-3} kg/m^{2}s. The comparison between experimental and simulation results was acceptable being the maximum difference of 11.1 and 28.4% for the absorber thermal load and the mass absorption flux, respectively.

Keywords: absorption; bubble absorber; ammonia-water; pleat heat exchanger; mass absorption flux

* Corresponding author. Tel. +52 686 566 41 50; Fax. +52 686 566 41 50.
E-mail address: jcerezo@iing.mxl.uabc.mx

Nomenclature

A	Heat transfer area, m^2
Ap	Projected Area, m^2
Cp	Heat capacity, kJ kg^{-1} K^{-1}

d	diameter, m
dam	Mass transfer area between liquid and the bubble, m^2
e	Wall thickness, m
g	gravity, m s^{-2}
h	Heat transfer coefficient, kW m^{-2} s^{-1}, specific enthalpy, kJ kg^{-1} K^{-1}
k	Thermal conductivity, kW m^{-1} K^{-1}
ke	Thermal conductivity, kJ m^{-1} s^{-1}
km	Mass transfer coefficient, kg m^{-2} s^{-1}
f	Darcy friction factor
L	Length, m
LMTD	Logarithmic mean temperature difference, K
m	Mass flow rate, kg s^{-1}
N	Mass Flux, kg m^{-2} s^{-1}
Nu	Nusselt number
P	Pressure, kPa
pd	Pressure drop, kPa
Pr	Prandtl number
Q	Heat, kW
q	Volumetric flow rate, m^3 s^{-1}
Re	Reynolds number
Sc	Schmidt number
Sh	Sherwood number
T	Temperature, °C
v	Velocity, m s^{-1}
x	Liquid ammonia concentration, % by weight
y	Vapor ammonia concentration, % by weight
z	Ratio of ammonia mass flux to the total mass flux, $kg_{\text{by weight}}$ $kg^{-1}_{\text{by weight}}$

Greek symbols

ρ	Density, kg m^{-3}

β	Diffusivity, $m^2\ s^{-1}$
μ	Dynamic viscosity, kg $m^{-1}\ s^{-1}$
σ	Surface tension N m^{-1}
λ	Latent heat, kW

Subscripts

AB	Absorber
B	Bubble
C	Cooling water
IN	Input
INT	Interface
O	Orifice
OUT	Output
S	Solution
SUB	Subcooling
TER	Terminal
V	Vapor
SEN	Sensible
NH3	Ammonia
H2O	Water

1. Introduction

Absorption cooling systems are attractive not only to industrial and commercial sectors but also to the residential one because they can be activated by low temperature heat sources such as waste heat, solar energy, etc., reducing then primary energy consumption. On the other hand, the low performance of these systems caused mainly by the absorption process results in bigger and heavier machines. The use of plate heat exchangers in the main components of these systems allows the enhancement of heat and mass transfer processes, which significantly reduces their overall size [1, 2].

Few researchers had developed different mathematical models in order to understand heat and mass transfer processes in ammonia-water bubble absorbers. Kang et al. [1] reported a mathematical model using a plate heat exchanger. The absorber was divided in control volumes based on the incremental of the section. They concluded that the vapor phase flow rate was the dominant parameter for heat transfer while the liquid phase flow rate was the dominant parameter for mass transfer. They also carried out a parametric analysis to determine the optimum design for the absorber. Herbine and Perez-Blanco [3] developed a mathematical model considering heat and mass transfer from the vapor to the solution, the authors defined a parameter called "vapor phase's extent" that defines the direction of absorption in the vapor phase in order to calculate the mass absorption flux. The authors presented the temperature and concentration profiles in the liquid and vapor phases along the absorber.

Kim et al. [4] added nano-particles and additives to the ammonia-water solution in order to improve the absorption process in a bubble absorber. Using the model proposed by Kang et al. [1], the authors concluded that surfactants and nano-particles enhance mass transfer and that their effect on heat transfer is much less pronounced being the absorber size reduction around 55%.

It's worthwhile remarking that both mathematical models developed by Kang et al. [1], Herbine and Perez-Blanco [3], and Kim et al. [4] were not validated using experimental data. Lee et al. [5] compared experimental data with numerical simulation results using a cylinder as bubble absorber. The authors concluded that the ammonia gas absorption is sensible to the quantity of input vapor, temperature and solution concentration and flow direction, also, the experimental values agreed with the simulation for the considered absorber operation conditions.

The objective of this paper is to compare a mathematical model developed for ammonia-water bubble absorbers with experimental data obtained in a corrugated heat plate exchanger at typical operation conditions of thermal cooling absorption systems. The results will allow the analysis of the effect of some important variables on the absorber performance, also some key parameters such as solution Nusselt number and Darcy factor will be presented.

2. Experimental methodology

2.1. Description of the experimental set-up

The experimental equipment consisted of a solution circuit and two secondary circuits (cooling and heating) as it is shown in Fig. 1. The poor solution (lower NH_3 concentration) stored in the solution tank (TS) was pumped and heated by the heat exchanger HX1 of the heating water circuit, until the set point of the inlet solution temperature was reached, then the solution entered at the bottom side of the absorber (ABS) and absorbed the ammonia vapor coming from the ammonia bottle (BA). The absorption heat generated was removed by the cooling water circuit. The rich solution (higher NH_3 concentration) leaves the absorber and enters to the vapor-liquid separator (SVL), where the ammonia vapor not absorbed in the absorber is separated from the solution and the rich solution is sent to the storage tank. Finally the rich solution is stored in storage tank (TA). More details about this experimental set-up can be found in references [6-7].

The plate heat exchanger used as absorber was manufactured by Alfa Laval (NB51 model, type L) and consisted of three channels of 0.1 m^2 effective surface area, where the solution flow rate enters in the central channel and cooling water flow rate enters in the side of absorber. Table 1 shows some geometry specifications of this plate heat exchanger.

2.2. Data reduction

Heat transfer coefficient correlation from experimental data

The conventional LMTD (eq. 1) was not used to calculate the solution heat transfer coefficient in the absorption process because the outlet cooling water temperature was higher than the inlet solution temperature in some experiments due to the heat of absorption, mainly with low cooling water flow rates.

$$\mathrm{LMTD} = \frac{(T_{S,IN} - T_{C,OUT}) - (T_{S,OUT} - T_{C,IN})}{\ln\left(\frac{T_{S,IN} - T_{C,OUT}}{T_{S,OUT} - T_{C,IN}}\right)} \quad (1)$$

This work proposes that LMTD should be calculated depending on the conditions of the solution flow rate. Two different conditions were obtained in these experiments: *Sub-vapor and vapor-vapor*.

The *Sub-vapor* (SUB-VAP) condition means that the inlet solution flow rate is at subcooling conditions and the outlet solution flow rate has a quantity of vapor. In this case, $T_{S,IN}$ (eq. 1) had sometimes in the experimental data a lower value than $T_{C,OUT}$, depending on the degree of subcooling or flow rate, resulting in problems with the heat transfer equation. For this reason, this inlet solution temperature is calculated in equilibrium condition from the inlet absorber pressure and concentration ($T_{S,EQ,IN}$) and LMTD is calculated using eq. 2.

$$\mathrm{LMTD} = \frac{(T_{S,EQ,IN} - T_{C,OUT}) - (T_{S,OUT} - T_{C,IN})}{\ln\left(\frac{T_{S,IN} - T_{C,OUT}}{T_{S,OUT} - T_{C,IN}}\right)} \quad (2)$$

The Nusselt number correlation (*Nu*) is calculated as a function of solution, cooling water, vapor Reynolds number, solution Prandtl number and pressure drop:

$$Nu = 0.01\,\mathrm{Re}_S^{\,0.37}\,\mathrm{Re}_C^{\,0.56}\,\mathrm{Re}_V^{\,-1.09}\,\mathrm{Pr}_S^{\,7.11}\,pd^{1.04} \quad (3)$$

The *vapor-vapor* (VAP-VAP) condition means that both inlet and outlet solution flow rates have a quantity of vapor. The calculation of LMTD is similar to equation 2, because there is no subcooling in the solution flow rate. Equation 4 shows the Nusselt number correlation for this condition:

$$Nu = 691.60\,\mathrm{Re}_S^{\,0.36}\,\mathrm{Re}_C^{\,-0.80}\,\mathrm{Re}_V^{\,0.10}\,\mathrm{Pr}_S^{\,-0.41}\,pd^{-0.19} \quad (4)$$

The two aforementioned conditions are near to saturation conditions

2.3. Pressure drop

The advantage of using plate heat exchangers is the higher heat transfer than that of a tube heat exchanger, however, they have a high pressure drop and both parameters are proportional, in other words, when heat transfer is increased, the pressure drop also increases. The pressure drop depends on the type of plate corrugation and the flow rate. The

Darcy friction factor correlation (eq. 5) was used to calculate the pressure drop. It can be applied for all range of experiments carried out in this work.

$$f = 492.75\,\mathrm{Re}_S^{-1.47}\,\mathrm{Re}_V^{0.22}\,\mathrm{Pr}_S^{-1.40} \quad (5)$$

The correlation presented above for heat transfer and pressure drop were obtained from experimental data from Cerezo [6] and they have a maximum error of 8% between experimental data and the values obtained from Nusselt number and Darcy friction correlations, and can be applied in the range of Re_S = 213-572, Re_C = 280-590, Re_V = 759-1994.

3. Bubble absorber modeling

The absorber modeling was carried out applying a numerical discretization that consisted in dividing the absorber into small control volumes along the absorber length, where liquid and vapor flow rates flow up in a co-current manner in the central channel while cooling water flows down in counter-current in the side channels as shown in Fig. 2a. A cooling water channel was eliminated in the model but keeping the same heat transfer area as shown in Fig. 2b. This assumption was made in order to simplify the heat dissipation calculations. The indices (i) and (i+1) means the input and output streams for each control volume (i). This mathematical model is based on those published by Kang et al. [1] and Herbine et al. [3].

3.1. Model assumptions

The model is based on the following suppositions:

- Absorption process is in steady state.
- Vapor and liquid phases are in equilibrium at the interface.
- Bubble velocity is constant.
- Vapor bubble has a spherical shape.
- There is no break-up and no interaction or coalescence amongst bubbles.

3.2. Governing equations

The mathematical model is based on energy and mass balances and the heat transfer equation (eq. 6) for each section; from these equations it is possible to calculate the values of the outlet variables using equations from 8 to 12, as it can be seen in Fig. 2b.

Q_{AB} = U A LMTD (6)

$$U = \frac{1}{\frac{1}{h_S} + \frac{e}{ke} + \frac{1}{h_C}} \quad (7)$$

$$Q_{AB} = Q_C = m_C Cp_C [T_C(i+1) - T(i)] \quad (8)$$

$m_V(i+1) + m_S(i+1) = m_V(i) + m_S(i) - (N_{NH3} + N_{H2O})$ dam (9)

$m_V(i+1)\ y(i+1) + m_S(i+1)\ x(i+1) = m_V(i)\ y(i) + m_S(i)\ x(i) - (N_{NH3}\ \text{dam})$ (10)

The liquid and vapor outlet were calculated from energy balances on their individual phases on the control volume with equation 11 and 12, respectively.

$m_V(i+1)\ h_V(i+1) = Q_{SEN,V} + m_V(i)\ h_V(i) - m_{NH3}\ h_{NH3,INT,V} - m_{H2O}\ h_{H2O,INT,V}$ (11)

$m_S(i+1)\ h_S(i+1) = Q_{SEN,S} - Q_C + m_S(i)\ h_S(i) + m_{NH3}\ h_{NH3,INT,S} + m_{H2O}\ h_{H2O,INT,S}$ (12)

3.3. Interfacial mass and energy balances

The mass and energy transferred in each control volume was calculated using the liquid and vapor phase diffusion equations (eq. 13 and 14) and solution and vapor sensible heats were calculated from eqs. 16 and 17.

$$N_{NH3} + N_{H2O} = km_L \ln\left(\frac{z - x}{z - x_{INT}}\right) \quad (13)$$

$$N_{NH3} + N_{H2O} = km_V \ln\left(\frac{z - y_{INT}}{z - y}\right) \quad (14)$$

$$cte_{S,V} = \frac{\frac{m_{NH3} Cp_{S,V,NH3} + m_{H2O} Cp_{S,V,H2O}}{h_{INT,S,V}}}{1 - e^{-\frac{m_{NH3} Cp_{S,V,NH3} + m_{H2O} Cp_{S,V,H2O}}{h_{INT,SV}}}} \left[h_{INT,S,V}\, dA_M\right] \quad (15)$$

$$Q_{SEN,S} = cte_{S,V}\left(T_{INT} - T_S\right) \quad (16)$$

$$Q_{SEN,V} = cte_{S,V}\left(T_V - T_{INT}\right) \quad (17)$$

An interfacial energy balance was calculated from equation 18

$$Q_\lambda = Q_{SEN,S} + Q_{SEN,V} \quad (18)$$

3.3.1. Heat and mass transfer coefficients

The solution and vapor heat transfer coefficients were calculated using a correlation obtained from Deckwer [8] and Clift [9], respectively. The solution and vapor mass transfer coefficients were calculated from Incropera [10] and Sherwood [11].

$$h_{INT,S} = 0.1\left(\frac{\rho_S v_V d_B}{\mu_S}\right)^{-0,25}\left(\frac{{v_V}^2}{g d_B}\right)^{-0,25}\left(\frac{\mu_S Cp_S}{k_S}\right)^{-0,5}\rho_S Cp_S v_V \quad (19)$$

$$h_{INT,V} = 1.4\frac{ACp_V}{A_P}\left(\frac{Sc_V}{\mathrm{Pr}_V}\right)^{\frac{2}{3}}\left(\frac{48\sigma{\beta_V}^2}{\pi^2 d_B \rho_S\left(2+3\rho_V/\rho_S\right)}\right)^{\frac{1}{4}} \quad (20)$$

$$Sh_{INT,S} = 2 + 0.0187\,\mathrm{Re}_B^{\,0.779}\,Sc_S^{\,0.546}\left(d_B g^{0.333}\beta_S^{-0.666}\right)^{0.116} \quad (21)$$

$$Sh_{INT,V} = 0.664\,\mathrm{Re}_B^{\,0.5}\,Sc_V^{\,1/3} \quad (22)$$

These coefficients were obtained from empirical equations and they represent the energy and mass transfer from the interface and the bulk zone.

3.3.2. Vapor velocity

Bubble velocity (v_B) was obtained from the sum of terminal (v_{TER}) and solution (v_S) velocity [10].

$$v_{TER} = \left(\frac{2.14\sigma}{\rho d_B} + 0.0505 g d_B\right)^{0.5} \quad (23)$$

$$v_B = 0.8\, v_{TER} + v_S \quad (24)$$

3.3.3. Initial Bubble diameter

The bubble size depends mainly on the orifice vapor velocity, orifice diameter, properties and turbulence of the fluid [12]. These correlations can be applied when turbulence is only generated by bubbles and orifices are in a horizontal position.

When $q_T < q_V$ then equation 25 can be applied

$$q_T = \left(\frac{20(\sigma d_O)}{g(\rho_S - \rho_V)^2 \rho_S{}^3} \right)^{1/6} \tag{25}$$

$$d_B = \left(\frac{6\sigma d_O}{g\rho_S} \right)^{\frac{1}{3}} \tag{26}$$

if $q > q_T$ and $Re_O < 2100$ then

$$d_B = 0.0287 d_O{}^{0.5} \, \mathrm{Re}_O{}^{1/3} \tag{27}$$

For $\mathrm{Re}_O = 10\,000$ to 50 000 and do = 0.4 – 1.6 mm:

$$d_B = 0.0071 \mathrm{Re}_O^{-0.05} \tag{28}$$

The bubble diameter correlations presented before were used at the first control volume. Final bubble diameter ($d_{B,F}$) was calculated from equation 29:

$$\frac{4}{3} \rho_V \pi \left(\frac{d_{B,F}}{2} \right)^3 n_B = m v_f \tag{29}$$

$d_{B,F}$ is the output bubble diameter (m) and it will be used to the initial bubble diameter for the next control volume, n_B is the number of bubbles, $m_{V,f}$ is final vapor flow rate (kg).

3.4. Solution Algorithm

The mathematical model has four dependent variables that have to be solved iteratively: z relation, interfacial temperature (T_{INT}), absorber thermal load (Q_{AB}), and inlet cooling water temperature [T_C(i)]. The first variable to iterate is the z relation as it is shown on block 5 and 6 of Fig. 3, the convergence is achieved when liquid and vapor diffusion equations are equal. The second variable is T_{INT} that converges when the interfacial heat balance is equal to the liquid sensible heat (block 8). Q_{AB} converges when the energy transfer equation and

heat balance are equal (block 10). Finally the solution is achieved when the assumed initial cooling temperature [$T_{C,A}(i)$] is equal to the calculated inlet cooling temperature [$T_C(i)$] as it is shown in blocks 1 and 12. Regarding the iterative approach, the secant method was used to solve the non linear equations that allow the calculation of the 4 unknown variables.

4. Results

Table 2 shows some results from the simulation (THEO) and experimental data (EXP) for a specific case of SUB-VAP and VAP-VAP conditions. $T_{S,IN}$ was calculated at saturated state for SUB-VAP condition in order to eliminate subcooling, but it is not possible to consider $T_{S,IN}$ at saturation state in VAP-VAP conditions, because the latent heat is large, then a saturation concentration should be calculated from inlet solution temperature and pressure. The injected vapor flow rate ($m_{V,IN}$) was higher than the ammonia absorbed flow rate (m_{AB}) in SUB-VAP and VAP-VAP conditions, therefore not all the ammonia vapor was absorbed in the absorber. Mass absorption flux ($\%F_{AB}$) and thermal load percent difference ($\%Q_{AB}$) between simulation and experimental data were around 28.4 and 8.7% respectively for SUB-VAP condition and 18.2 and 6.2% for VAP-VAP condition. Thermodynamic properties such as enthalpy, density, temperature, concentrations were calculated from correlations obtained from Ibrahim [13].

4.1. Parametric analyses of the absorber performance

The comparison of simulation versus experimental data on pressure drop, cooling flow rate, solution flow rate, absorber pressure, solution concentration, solution temperature and cooling water is presented in this section.

Analysis of pressure drop and cooling flow rate

Figure 4 shows the comparison of pressure drop on mass absorption flux and thermal load with simulation and experimental data as a function of cooling water flow rate. When the cooling water flow rate increases, the mass absorption flux (F_{AB}) from experimental data also increases from 0.0036 to 0.0047 kg/m^2 s with a pressure drop of 9 kPa (empty circle). Mass absorption flux is around 20.5% lower for the simulation results than experimental

data. When pressure drop is null from simulation (empty square), F_{AB} has similar values than experimental data. Moreover, pressure drop has no significant effect on the absorber thermal load; this may be caused by the heat transfer coefficient correlation obtained from experimental data, while the mass transfer coefficient correlation was obtained from published data.

Figures 5 and 6 show the comparison of cooling water flow rate on mass absorption flux and absorber thermal load from simulation and experimental data at solution flow rate of 30 kg/h. Simulation and experimental data show similar trends for mass absorption flux (F_{AB}) and absorber thermal load (Q_{AB}). F_{AB} increases from 0.0036 to 0.0047 kg/m^2 s and Q_{AB} from 0.72 to 0.97 kW, as the cooling water Reynolds number (Re_C) is increased from 280 to 517. The simulation values have a lower value than the experimental data and they have a maximum error of 28.4% and 10.3% for F_{AB} and Q_{AB}, respectively.

Analysis of solution flow rate and absorber pressure

Figures 7 and 8 show the comparison of absorber pressure on the mass absorption flux and the heat load as a function of solution flow rate with simulation and experimental data at different absorber pressure. When the solution flow rate increases, the mass absorption flux from experimental data increases linearly from 0.0025 to 0.0029 kg/m^2 s at 162 kPa while the absorber thermal load increases linearly from 0.52 to 0.71 kW. F_{AB} and Q_{AB} have an average percent difference between simulation and experimental data of 13 and 12 % at 202 kPa and 19 and 7% at 162 kPa, respectively.

Analysis of solution concentration

Figures 9 and 10 compare the effect of solution concentration on F_{AB} and Q_{AB} with simulation and experimental data as a function of the solution Reynolds number. When inlet absorber concentration (x_{AB}) decreases from 33 to 29 wt.%, the mass absorption flux is increased from 0.0025 to 0.0043 kg/m^2 s and Q_{AB} from 0.51 to 0.98 at solution Re_S = 210. F_{AB} was increased from 0.0027 to 0.0049 kg/m^2 s and Q_{AB} increases from 0.64 to 1.2 kW at solution Re_S = 365 from experimental data. It was caused mainly by the increase of

driving concentration between ammonia vapor and solution concentration at the absorber entrance. F_{AB} and Q_{AB} have a maximum of 13 percent difference between simulation and experimental at 29 wt.%, while F_{AB} and Q_{AB} have and average difference value of 19 % and 7%, respectively at 33 wt.%.

Analysis of solution temperature

Figures 11 and 12 compare the effect of solution temperature on F_{AB} and Q_{AB} with simulation and experimental data as a function of the solution Reynolds number. The difference between simulation and experimental are very similar for flux absorber from 0.0036 to 0.0043 kg/m^2 s (13% average error) at 38ºC, but this difference (24%) is higher at 42ºC. This is because the injected vapor flow rate was higher in experiments than in the simulation due to the limited range of validity for the bubble diameter correlation.

Absorber thermal load ($Q_{AB)}$ has a lineal increase from 0.86 – 1.17 kW at T_S = 38ºC and 0.95 – 1.27 kW at T_S = 42ºC from experimental data. The simulation has a good tendency with respect experimental with a maximum average error of 12%.

Analysis of cooling water temperature

Figures 13 and 14 show the mass absorption flux and the absorber thermal load as a function of solution Reynolds number at different cooling water temperatures. These figures show that the simulation and experimental data have very similar tendencies and values. Absorber thermal load and mass absorption flux obtained values from 0.4 to 1.27 kW and 0.0016 to 0.0055 kg/ m^2 s, respectively.

5. Conclusions

A bubble absorber mathematical model was described considering heat and mass transfer from the bubble to the cooling water and was compared with experimental data obtained with a corrugated plate heat exchanger used as absorber. The following conclusions result from the work carried out:

- A logarithmic mean temperature difference (LMTD) was proposed for the heat transfer equation in the absorber, considering the solution at the absorber inlet at saturation conditions.
- Correlations, based mainly on the inlet flow rates, were developed for the heat transfer coefficient and Darcy factor from experimental data for a plate heat exchanger, model NB51. The maximum difference was around 8% for both heat transfer coefficient and pressure drop correlations.
- The increase of cooling water and solution flow rates and pressure had positive effect on the absorption performance, but the increase of concentration, cooling water temperature and solution temperature affected it negatively.
- Absorber thermal load and mass absorption flux were compared with the mathematical model and experimental data at different pressure drop, pressure, cooling and solution flow rate, solution concentration and cooling water and solution temperature. The comparison gave good results with experimental data. The maximum error obtained were 11.1 % for Q_{AB} and 28.4% for $F_{AB.}$ F_{AB} and Q_{AB} results could be improved if a specific mass transfer correlation for NH_3-H_2O were available.
- The results show that the mathematical model developed can simulate with good accuracy the absorption process in a plate heat exchanger in bubble mode and that it could be used as a useful tool to design a compact absorption system.

References

[1] Y.T. Kang, R.N. Christensen, T. Kashiwagi, Ammonia–water bubble absorber with a plate heat exchanger, ASHRAE Trans. 104 (1998) 1565-1576.

[2] K.B. Lee, B.H. Chung, J.C. Lee, C.H. Lee and S.H. Kim, Experimental analysis bubble mode in a plate-type absorber, Chem. Engineering Sc, 57 (2002) 1923-1929.

[3] G. S. Herbine, H. Perez-Blanco, Model of an ammonia-water bubble absorber. ASHRAE Transactions, 101 (6) (1995) 1324-1332.

[4] J-K. Kim, J.Y. Jung, Y.T. Kang, The effect of nano-particles on the bubble absorption performance in a binary nanofluid, International Journal of Refrigeration. 29 (2006) 22-29.

[5] J. Lee, K. Lee, B. Chun, C. Lee, J.J. Ha, S.H. Kim, A study on numerical simulations and experiments for mass transfer in bubble mode absorber of ammonia and water, International Journal of Refrigeration, 26 (2003) 551–558.

[6] J. Cerezo, Estudio del proceso de absorción con amoníaco-agua en intercambiadores de placas para equipos de refrigeración por absorción. PhD Thesis, Universitat Rovira i Virgili, Tarragona, Cataluña, Spain, 2006.

[7] J. Cerezo, M. Bourouis, M. Vallès, A. Coronas, R. Best, Experimental study of an ammonia-water absorber using a plate heat exchanger for absorption refrigeration machines, Applied Thermal Engineering 29 (2009) 1005-1011.

[8] W.D. Deckwer, On the mechanism of heat transfer in bubble column reactor, Chemical Engineering Science, 35 (1980) 1341-1349.

[9] R. Clift, J.R. Grace and M.E. Weber, Bubbles, drops and particles, New York: Academic Press, 1978.

[10] F.P. Incropera, D. P. De Witt, Fundamental of Heat and Mass Transfer, Ed. 3rd, John Wiley & Sons cop., New York, 1990.

[11] T. K. Sherwood, R. L. Pigford, C.R. Wlke, Mass Transfer, Mc Graw-Hill, New York, 1975.

[12] R. E. Treybal, Mass Transfer Operations, 3ra edition, McGraw-Hill, 1981.

[13] O. M. Ibrahim, S.A. Klein, Thermodynamic properties of ammonia-water mixtures, ASHRAE Trans: Symposia, 99 (1993) 1495-1502.

CAPTION LEGENDS

Fig. 1. Schematic diagram of the experimental set-up.

Fig. 2. Absorber control volume.

Fig. 3. Algorithm for resolution of the mathematical model.

Fig. 4. Mass absorption flux and absorber thermal load as a function of cooling Reynolds number with or without pressure loss.

Fig. 5. Mass absorption flux as a function of cooling water Reynolds number at different solution flow rate.

Fig. 6. Absorber thermal load as a function of cooling water Reynolds number at different solution flow rate.

Fig. 7. Effect of solution Reynolds number and pressure on the mass absorption flux.

Fig. 8. Effect of solution Reynolds number and pressure on the absorber thermal load.

Fig. 9. Effect of input solution concentration on the mass absorption flux.

Fig. 10. Effect of input solution concentration on the absorber thermal load.

Fig. 11. Effect of input solution temperature on the mass absorption flux.

Fig. 12. Effect of input solution temperature on the absorber thermal load.

Fig. 13. Effect of input cooling temperature on mass absorption flux.

Fig. 14. Effect of input cooling temperature on absorber thermal load.

Table 1. Plate heat exchanger geometry

Table 2. Comparison between experimental data and mathematical model results for each condition.

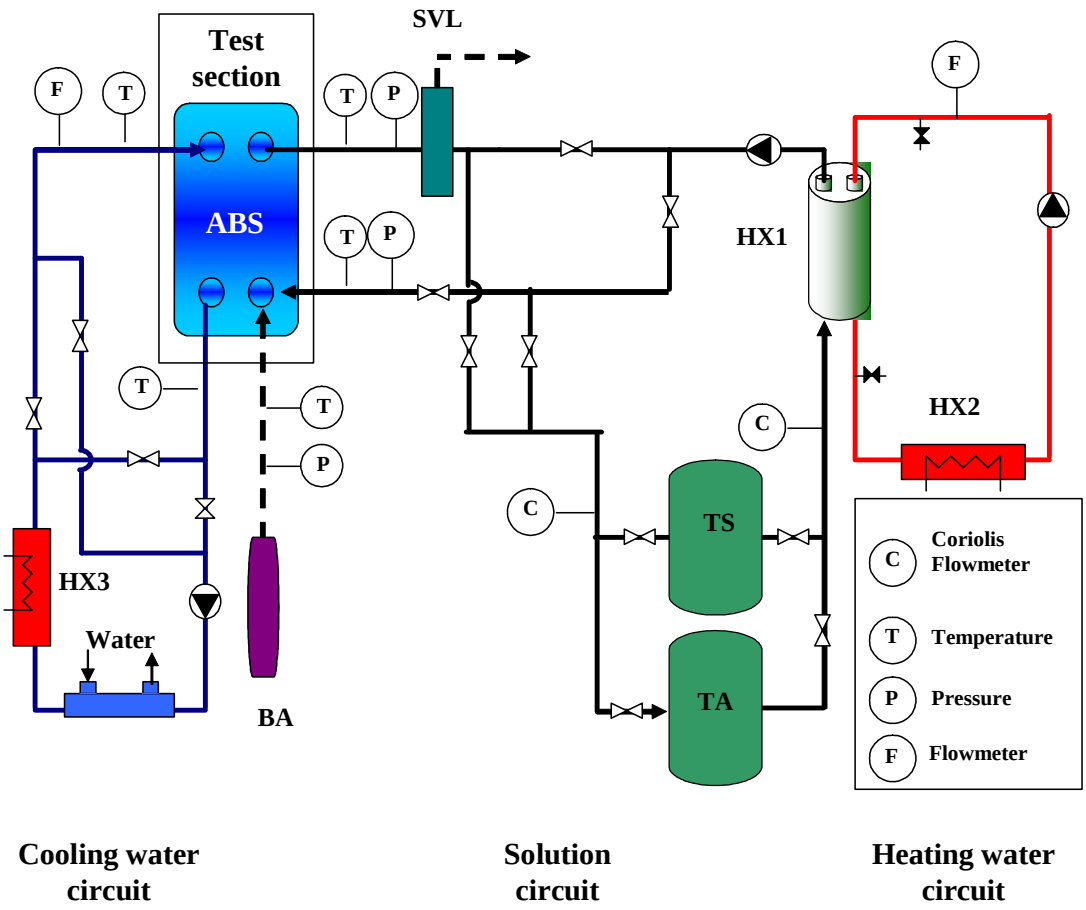

Fig. 1. Schematic diagram of the experimental set-up.

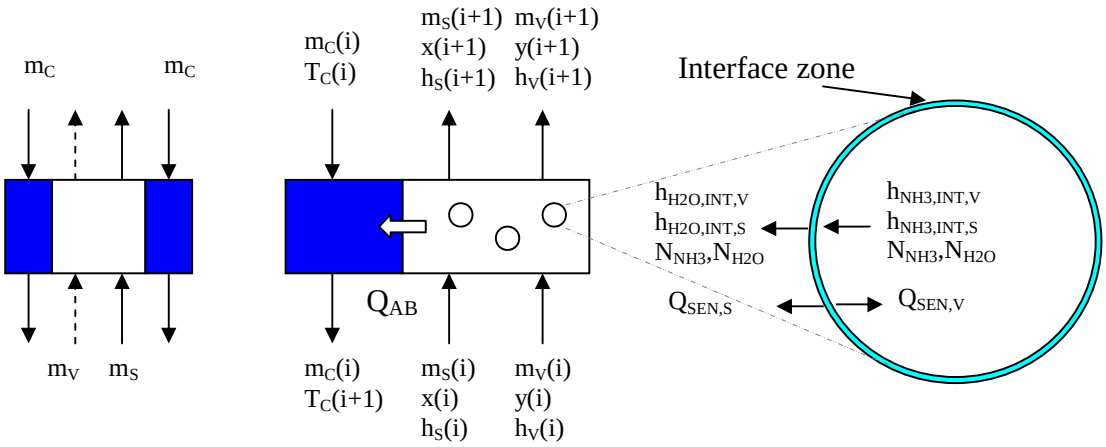

Fig. 2. Absorber control volume.

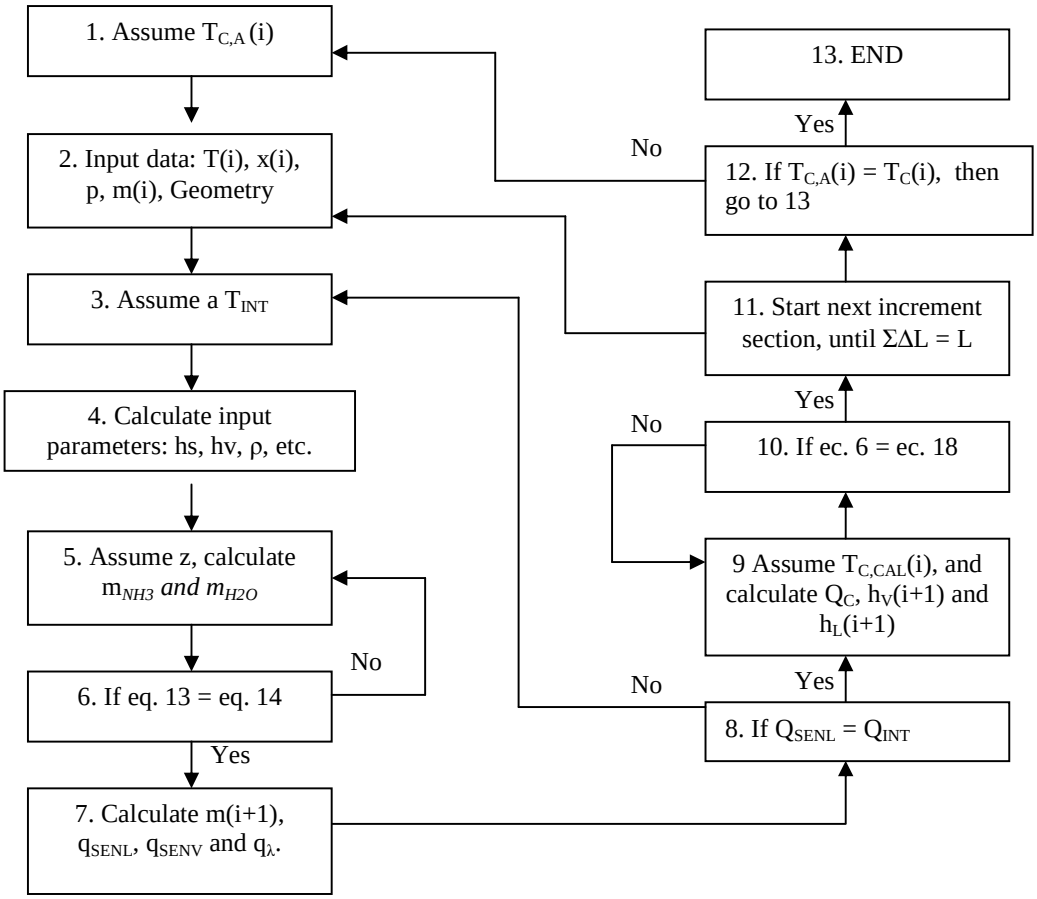

Fig. 3. Algorithm for resolution of the mathematical model.

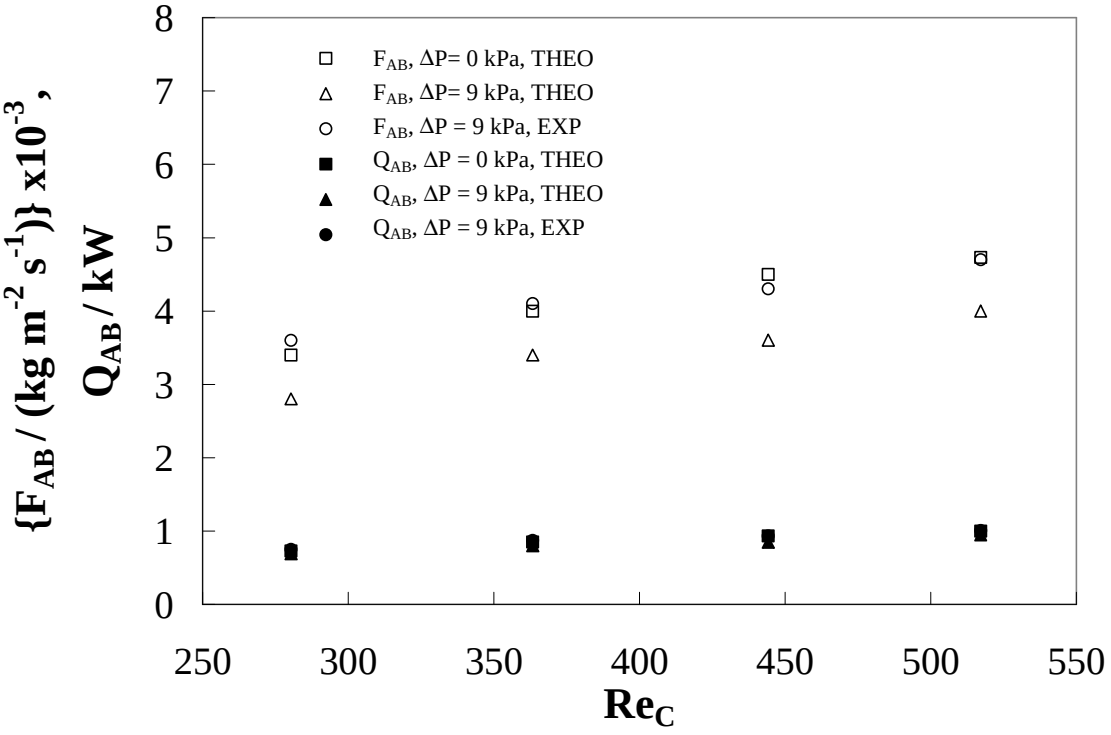

Fig. 4. Mass absorption flux and absorber thermal load as a function of cooling Reynolds number with or without pressure loss.

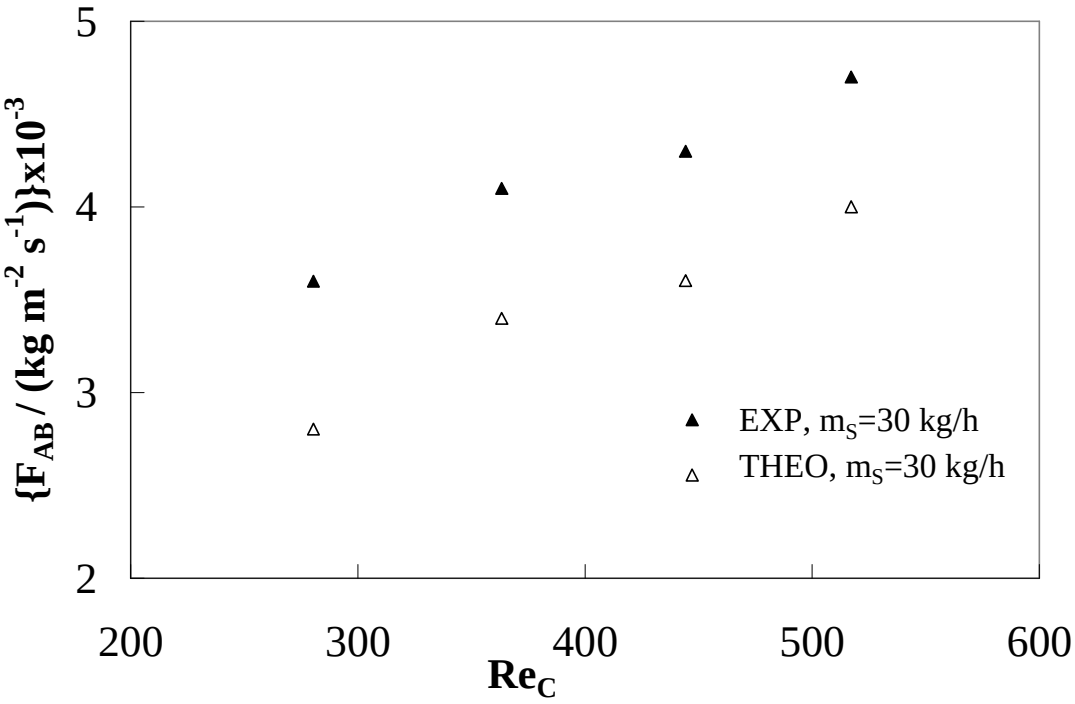

Fig. 5. Mass absorption flux as a function of cooling water Reynolds number at different solution flow rate.

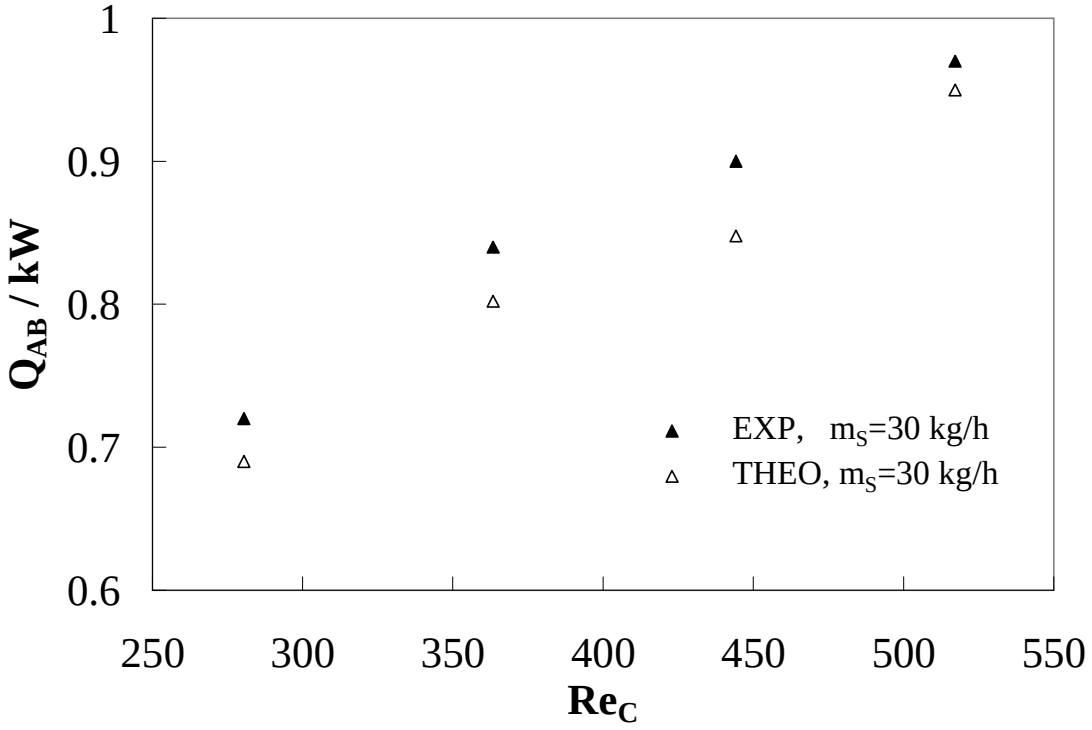

Fig. 6. Absorber thermal load as a function of cooling water Reynolds number at different solution flow rate.

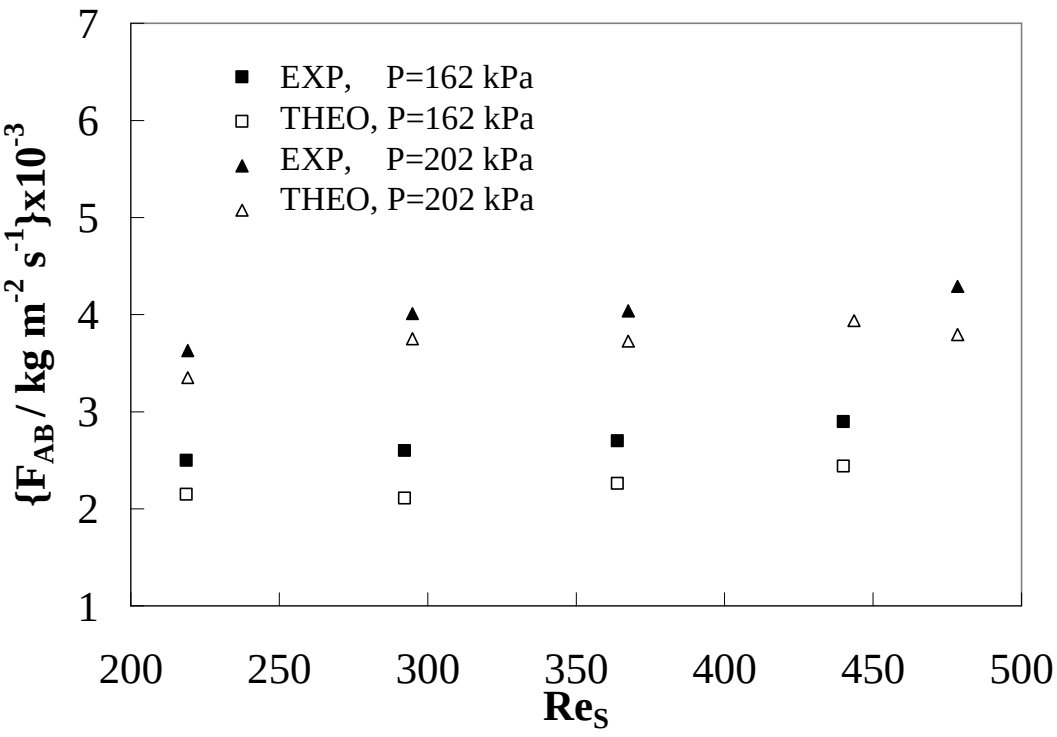

Fig. 7. Effect of solution Reynolds number and pressure on the mass absorption flux.

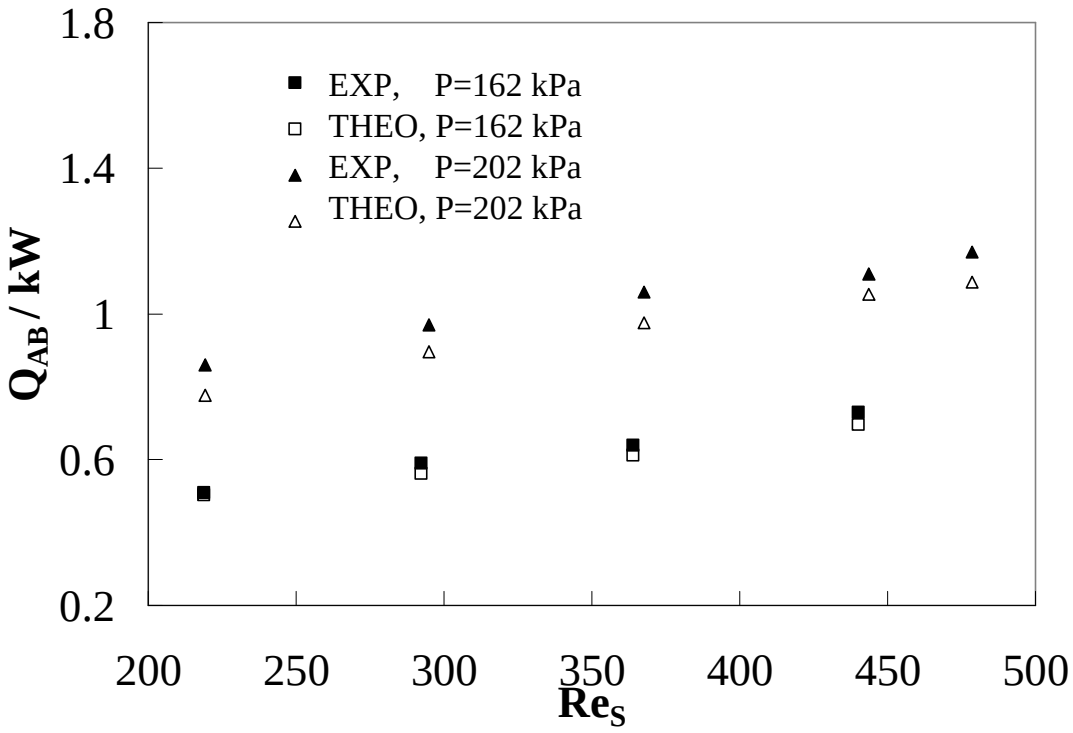

Fig. 8. Effect of solution Reynolds number and pressure on the absorber thermal load.

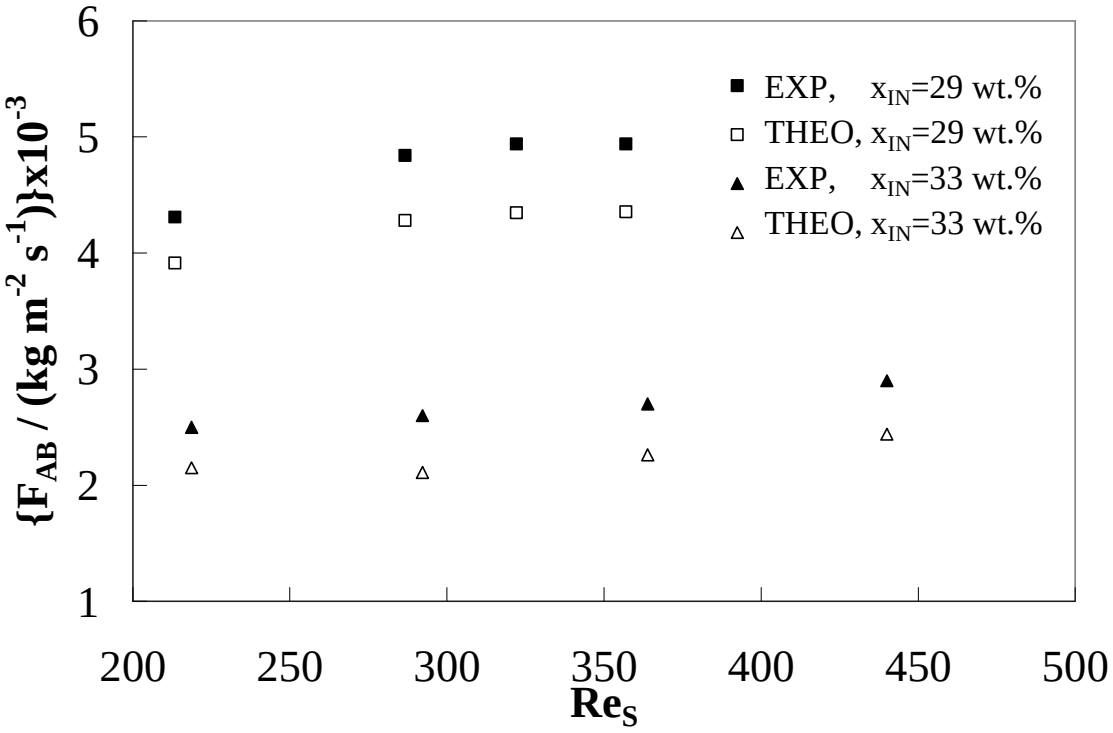

Fig. 9. Effect of input solution concentration on the mass absorption flux.

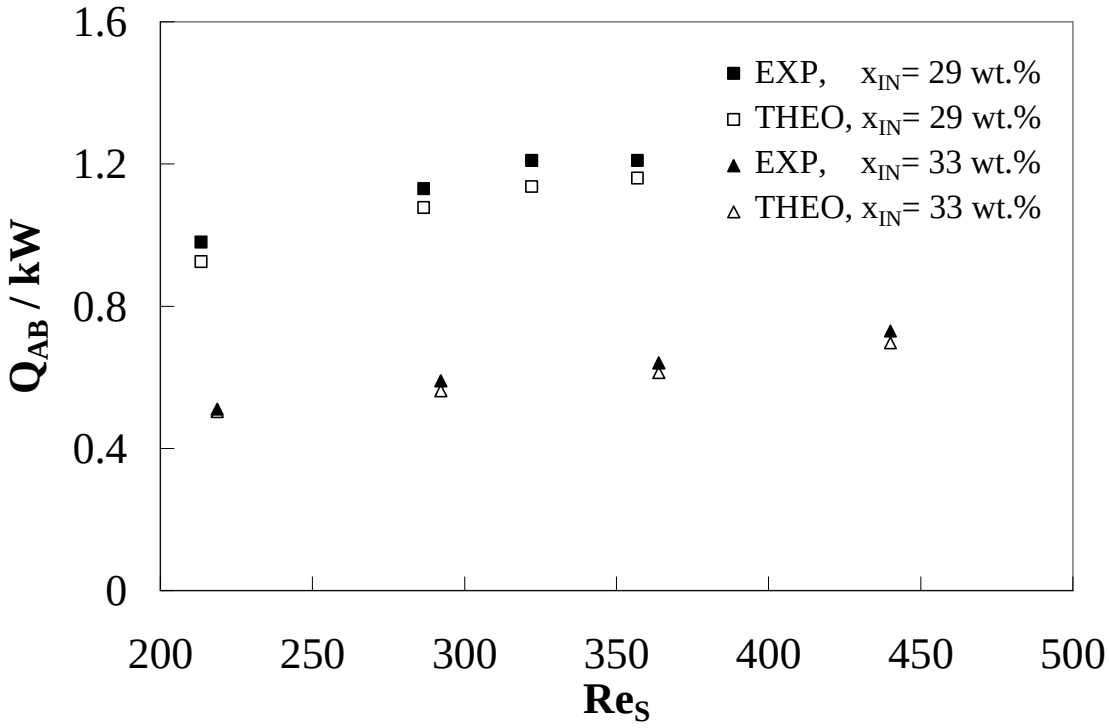

Fig. 10. Effect of input solution concentration on the absorber thermal load.

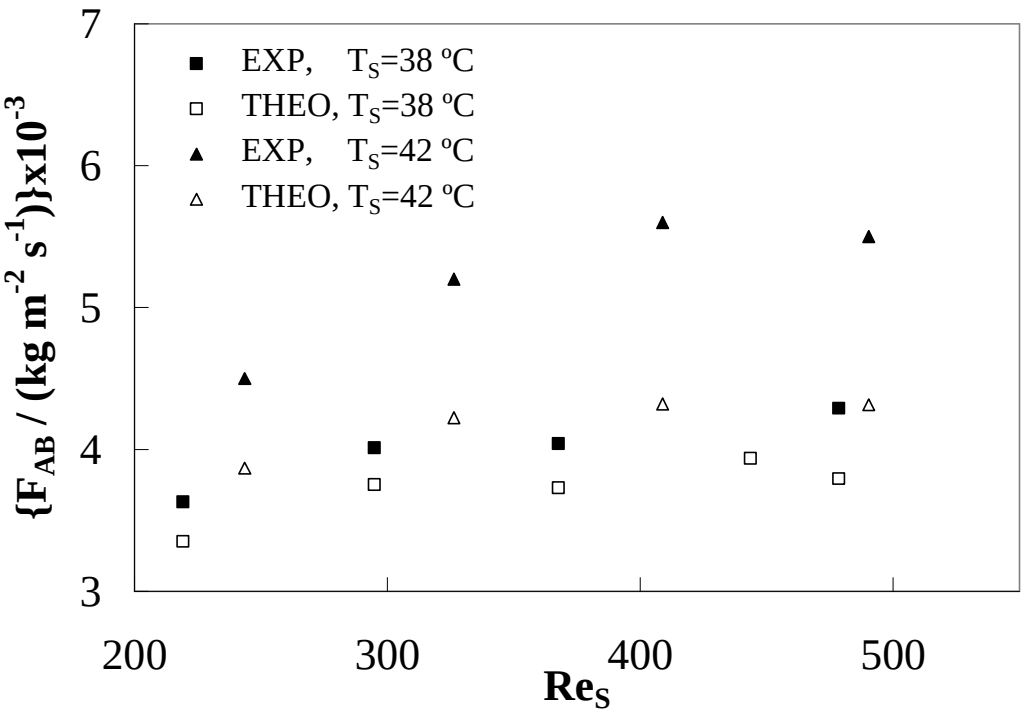

Fig. 11. Effect of input solution temperature on the mass absorption flux.

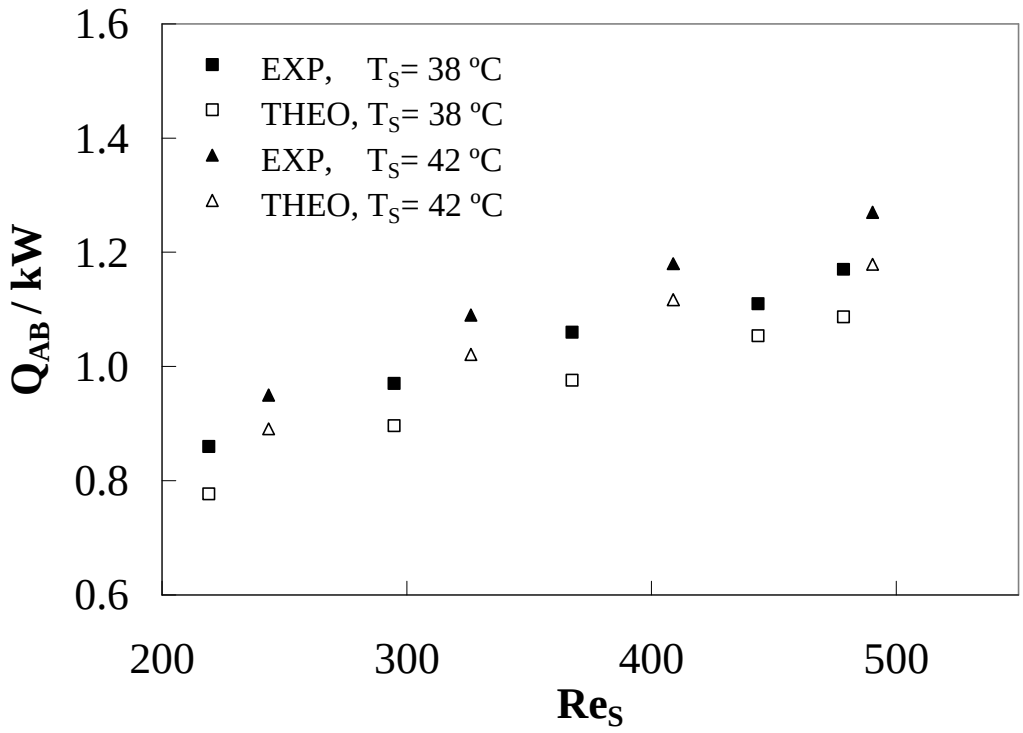

Fig. 12. Effect of input solution temperature on the absorber thermal load.

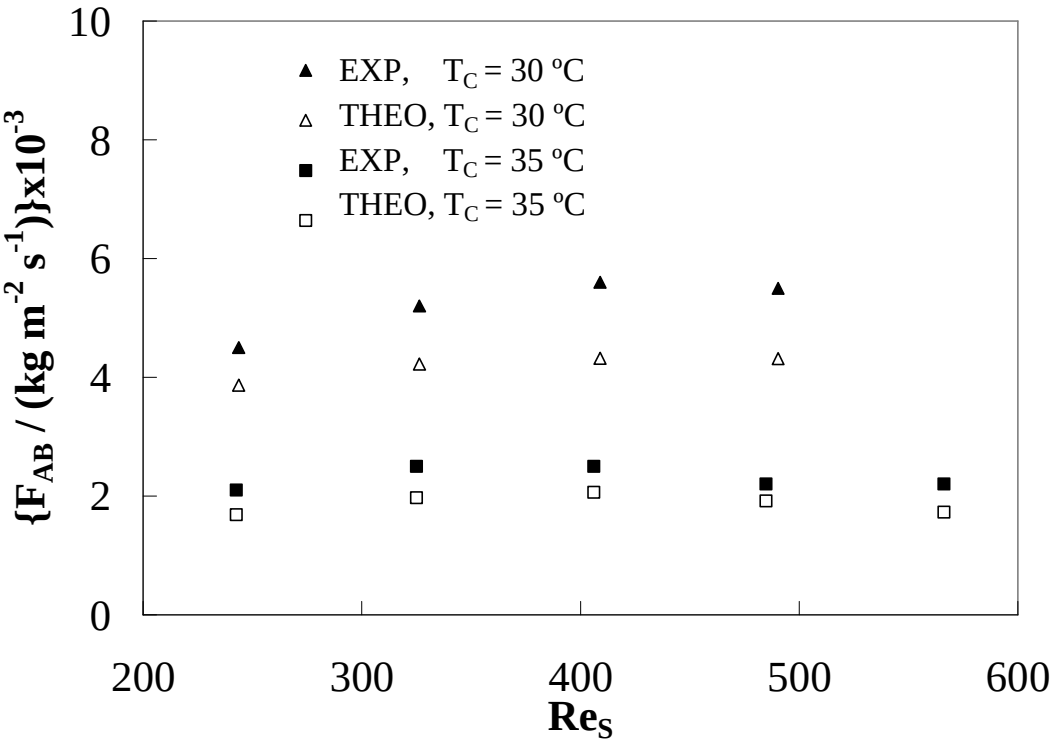

Fig. 13. Effect of input cooling temperature on mass absorption flux.

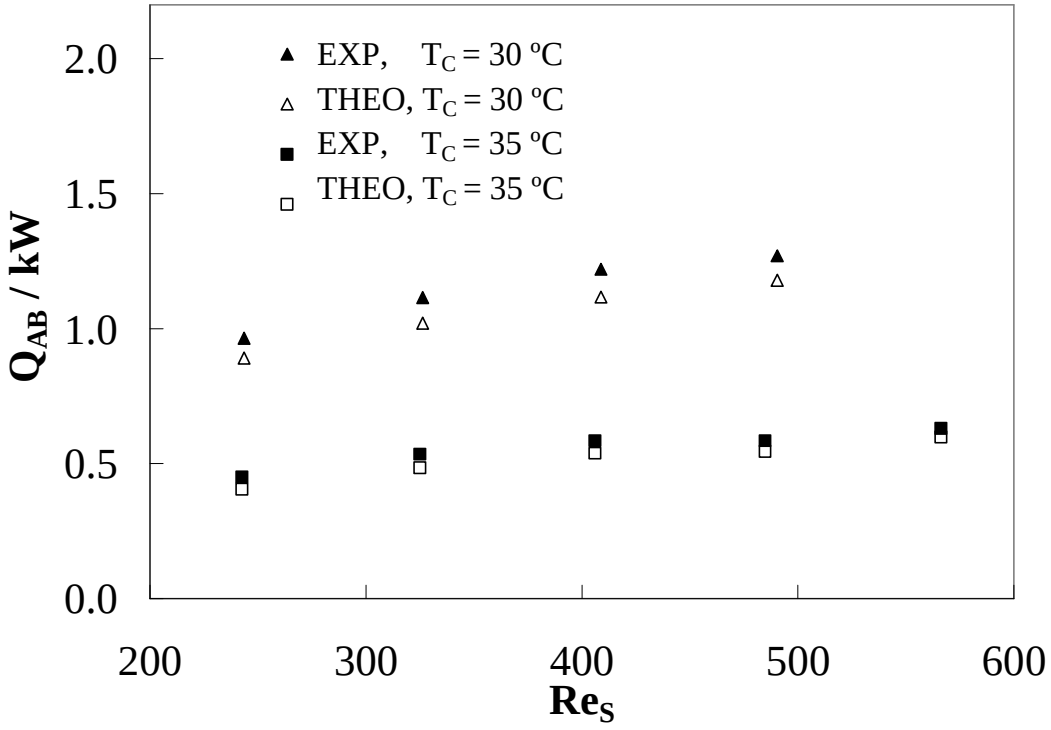

Fig. 14. Effect of input cooling temperature on absorber thermal load.

Table 1

Plate heat exchanger geometry

Geometry	Value
Heat transfer area, m^2	0.5
Length, m	0.5
Width, m	0.1
Pinch, m	0.002

Table 2

Comparison between experimental data and mathematical model results for each condition.

Parameter	**SUB-VAP**		**VAP-VAP**	
	EXP	**THEO**	**EXP**	**THEO**
$\mathbf{T_{S,IN}}$, **ºC**	37.7	41.6	37.7	37.7
$\mathbf{T_{S,OUT}}$, **ºC**	35.3	34.7	33.3	33.0
$\mathbf{T_{C,IN}}$, **ºC**	30.1	30.2	30.1	30.1
$\mathbf{T_{C,OUT}}$, **ºC**	38.5	38.0	34.6	34.4
$\mathbf{T_{V,IN}}$, **ºC**	-3.8		-3.7	
$\mathbf{x_{IN}}$, **wt. %**	33.36		33.9	
$\mathbf{x_{OUT}}$, **wt. %**	35.86	35.55	34.93	33.91
$\mathbf{Re_S}$	220		440	
$\mathbf{Re_C}$	280		502	
$\mathbf{m_{V,IN}}$, **kg/s**	0.00046		0.00053	
$\mathbf{m_{AB}}$, **kg/s**	0.00036	0.00028	0.00029	0.00024
$\mathbf{Q_{AB}}$, **kW**	0.75	0.69	0.74	0.70
% $\mathbf{F_{AB}}$	28.40		18.80	
% $\mathbf{Q_{AB}}$	8.65		6.25	